Available online at www.sciencedirect.com
SCIENCE DIRECT®
Journal of Solid State Chemistry 177 (2004) 3281–3289
JOURNAL OF SOLID STATE CHEMISTRY
http://elsevier.com/locate/jssc

Oxidation process of MoO_xC_y to MoO_3: kinetics and mechanism

L.O. Aleman-Vázquez,[a,b] E. Torres-García,[a,*] G. Rodríguez-Gattorno,[c] J. Ocotlán-Flores,[d] M.A. Camacho-López,[d] and J.L. Cano[a]

[a] *Instituto Mexicano del Petróleo, Eje Lázaro Cárdenas 152, Programa de Investigacion y Desarrollo de Crudo Maya, San Bartolo Atepehuacan México D.F. 07730, Mexico*

[b] *Universidad Auótnoma del Estado de Hidalgo, Carr. Pachuca-Tulancing Km. 4.5, Pachuca, Hgo. Mexico*

[c] *Departamento de Química Inorgánica y Nuclear, Facultad de Química, Universidad Nacional Autónoma de México, Coyoacán, México D.F. 04510, Mexico*

[d] *Centro de ciencias Aplicadas y Desarrollo Tecnológico, Universidad Nacional Autónoma de México, Apdo. Postal 70–186, Cd Universitaria, México D.F. 04510, Mexico*

Received 12 December 2003; received in revised form 22 April 2004; accepted 17 May 2004

Available online 20 July 2004

Abstract

A non-isothermal kinetic study of the oxidation of "carbon-modified MoO_3" in the temperature range of 150–550°C by simultaneous TGA–DTA was investigated. During the oxidation process, two thermal events were detected, which are associated with the oxidation of carbon in MoO_xC_y and MoO_2 to MoO_3. The model-free and model-fitting kinetic approaches have been applied to TGA experimental data. The solid state-kinetics of the oxidation of MoO_xC_y to MoO_3 is governed by F1 (unimolecular decay), which suggests that the reaction is of the first order with respect to oxygen concentration. The constant $(Ea)_\alpha$ value (about 115 ± 5 kJ/mol) for this first stage can be related to the nature of the reaction site in the MoO_3 matrix. This indicates that oxidation occurs in well-defined lattice position sites (energetically equivalent). On the other hand, for the second stage of oxidation, MoO_2 to MoO_3, the isoconversional analysis shows a complex $(Ea)_\alpha$ dependence on (α) and reveals a typical behavior for competitive reaction. A D2 (two-dimensional diffusion) mechanism with a variable activation energy value in the range 110–200 kJ/mol was obtained. This can be interpreted as an inter-layer oxygen diffusion in the solid bulk, which does not exclude other simultaneous mechanism reactions.
© 2004 Elsevier Inc. All rights reserved.

Keywords: Molybdenum oxycarbide; MoO_3; Isoconversion method; Kinetics oxidation; Kinetics in solid; Thermal analysis

1. Introduction

The molybdenum oxycarbide (MoO_xC_y) system has recently received much attention because of its good combination of activity and selectivity for isomerization reactions of saturated hydrocarbons at the expense of the cracking reactions [1–3]. These oxides have been extensively employed in industrial applications and in academic research. However, since the structure of the active surface is still not fully understood, the properties of a large variety of molybdenum-containing systems have been studied in detail in order to elucidate their catalytic behavior [4–6].

Molybdenum oxycarbide can be prepared directly from the oxide, MoO_3. Under appropriate condition reduction at low temperature (350°C) and a mixture of H_2/n-C_7, MoO_3 can produce different phases, one of which is the oxycarbide of molybdenum (MoO_xC_y) [1,4,5]. Since the reduction of MoO_3 is a crucial step in the activation of catalytic isomerization reactions, the reduction process with n-C_7 and hydrogen has been extensively studied. The formation of partially reduced molybdenum "carbon-modified MoO_3" during this reaction has been reported as a result of its redox behavior [4,7,8]. Regardless of the extensive studies on MoO_3 little attention has been focused on molybdenum oxycarbide obtained during the catalytic reduction of the pure oxide. It is important to remark that the hydrocarbon catalytic conversion, which is the main

*Corresponding author. Fax: 52-9175-8429.
E-mail address: etorresg@imp.mx (E. Torres-García).

0022-4596/$ - see front matter © 2004 Elsevier Inc. All rights reserved.
doi:10.1016/j.jssc.2004.05.035

application of MoO_3, appears to proceed in the presence of a carbonaceous layer (carbon modified molybdenum oxide); the understanding of the properties of this layer, then, is a key to a full understanding of hydrocarbon conversion reactions. In addition, the study of the oxidation of the catalyst bulk oxide is a crucial step in the redox mechanism and a very important contribution to the possibility of recovering the catalyst properties of MoO_3. For this reason, in order to obtain a more detailed analysis of the evolution of the "carbon-modified MoO_3" structure, kinetic studies on the oxidation process of MoO_xC_y to MoO_3 require special attention. Here, kinetic studies on the non-isothermal oxidation of MoO_3-reduction products in dry air at temperatures between 150°C and 600°C are presented, employing simultaneous thermal analysis TGA–DTA. For this purpose the model free method (isoconversion) and the model-fitting method $f(\alpha)$ were employed. The results are discussed in terms of the relationship between activation energy and the most probable mechanisms. A mixture of H_2/n-C_7 was used to simulate the MoO_3 reduction that takes place during the catalytic isomerization process.

2. Experimental

2.1. Sample and methodology

Molybdenum oxycarbide was obtained directly from the oxide MoO_3 (99.5%, Aldrich) with 4 μm particle size and superficial area of 0.7096 m^2/g, at low temperature (370°C) in a mixture of H_2/n-C_7 (39/1) at medium pressure.

The samples were characterized by means of X-ray diffraction using a Siemens diffractometer (Model D5000) with Cu$K\alpha$ radiation and a Ni filter. The operating conditions were 30 kV and 20 mA in the angular range 4–70° in 2θ. Crystalline phase identification based on XRD patterns was aided by the ICDD-PDF-2 database.

The Raman spectra of MoO_3 and MoO_xC_y at different times were obtained in air at room temperature with a double monochromator Raman spectrometer (SPEX Mod. 1403) using an Ar^+ ion laser which delivered 10 mW of incident radiation. The excitation line of the laser was 514.5 nm. The Raman signal was detected with a photomultiplier and a standard photon counting system.

Thermal analysis were made with a JUPITER NETSCH STA 449C apparatus, using an atmosphere of ultra dry air and flow of 50 mL/min. The programmed heating rates were 0.5, 1.5, 2.5 and 5°C/min. The sample weight was approximately 30.5 mg in all cases.

3. Results and discussion

3.1. Structural transformation of MoO_3 into MoO_xC_y

3.1.1. X-ray diffraction

XRD patterns of the starting oxide (MoO_3) and samples of MoO_xC_y obtained by reduction with a mixture of H_2/n-C_7 at 370°C after 4 and 10 h are present in Fig. 1. Furthermore, in the same figure the X-ray of the sample obtained during re-oxidation process of a MoO_xC_y has been included. For the initial MoO_3, narrow diffraction lines corresponding to MoO_3 were detected (JCPDS data file no. 05–0508). The intensities of the $\{0k0\}$ diffraction lines were anomalously high. This is due to the structure of MoO_3, which is formed by layers of $[MoO_6]$ octahedrons, stacked along the [010] direction, which favors platelet crystallites with a preferential orientation along this axis. After 4 h under flow of the H_2/n-C_7 mixture, the X-ray diagram obtained from the sample indicated the presence of two new phases besides MoO_3. These phases are unequivocally related to MoO_2 and "carbon-modified MoO_3" structure, the latter having interplanar distances d at 0.61798, 0.3059 and 0.2040 nm (Fig. 1), which is similar to previous reports [5,9]. The carbon-modified MoO_3 can be interpreted from a structural point of view as a result of the contraction of the distances between the planes of MoO_6 octahedrons, bound together by van der Waals interactions in the direction [010], motivated

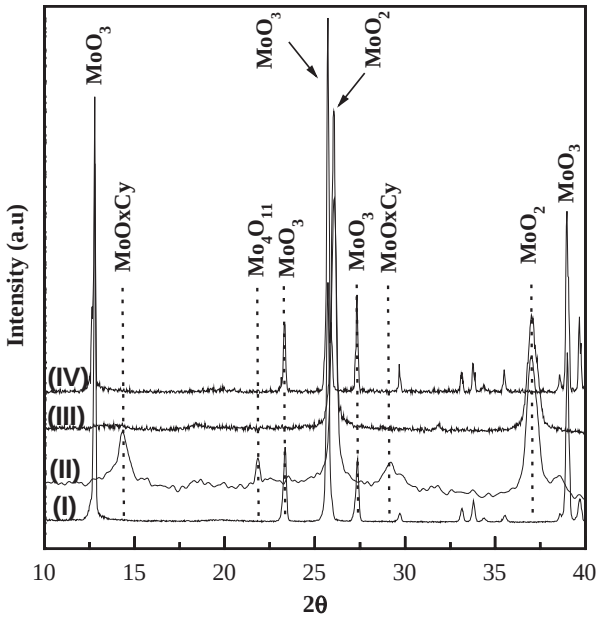

Fig. 1. XDR patterns of the molybdenum oxide samples, (I) MoO_3 (orthorhombic system JC-PDF2-No. 05–0508), (II) MoO_xC_y after 4 h, (III) MoO_2 (JCPDS data file no. 32–671) after 10 h both obtained with reductive mixture of H_2/n-C_7 at 370°C and, (IV) MoO_3 obtained during re-oxidation process.

by simultaneous reduction and the substitution of oxygen atoms with carbon atoms to form the MoO_xC_y. This suggests that the planes of MoO_xC_y are reminiscent of the MoO_3 planes. The XRD diagram for the sample after 10 h under flow of the reducing mixture shows the presence of only MoO_2 (JCPDS data file no. 32–671). Therefore, the formation of critical concentration of oxygen vacancies on the (010), (100) and (001) planes and incorporation of carbon in the MoO_3 matrix during the reducing treatment promotes lattice collapse and its reorganization into MoO_2 structure [1,5].

The low intensity reflection at 22° (2θ) corresponds to residues of the well-known Mo_4O_{11} phase, which is an intermediary of the MoO_3 hydrogen reduction [9].

3.1.2. Raman spectroscopy

In Fig. 2, four selected Raman spectra of MoO_3 and MoO_xC_y at 4, 6 and 10 h are shown. Raman bands at 471, 666, 820 and 996 cm^{-1} correspond to orthorhombic MoO_3, while bands at 461, 495, 571, 589 and 744 cm^{-1} are characteristic of monoclinic MoO_2 obtained during the experiments, which is in agreement with our XRD results and previous work [10,11].

Fig. 2 shows the evolution of the Raman spectra at different reaction times of the reduction process of the MoO_3 phase and its conversion into MoO_2. The bands at 820 and 996 cm^{-1} significantly decreased in intensity and resolution as the reaction time is increased. Moreover, Fig. 2 illustrates that (MoO_xC_y) phase is highly disordered, which is in agreement with X-ray results

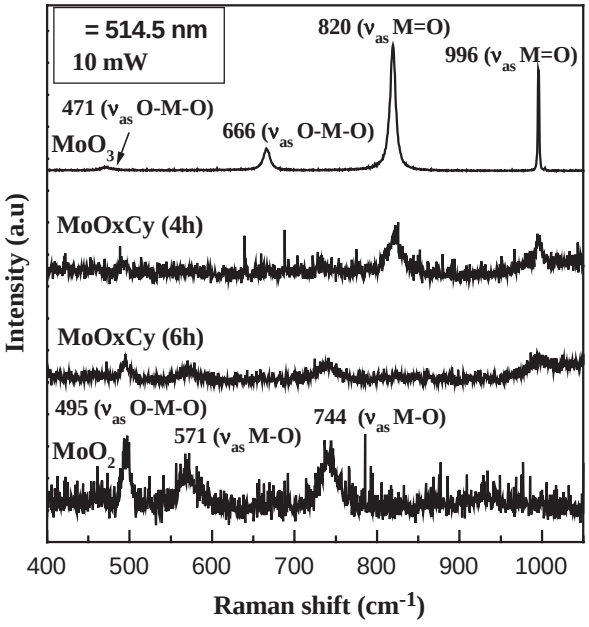

Fig. 2. Characteristic Raman spectra for different samples: (I) MoO_2 after 10 h, (II) and (III) MoO_xC_y after 6 and 4 h of the reaction under reductive mixture of H_2/n-C_7 at 370°C and (IV) starting metal oxide (MoO_3).

(Fig. 1); this is due to the increase of oxygen defects and the incorporation of carbon in the oxide matrix (MoO_3). An increase, of oxygen vacancy concentration and the degree of substitution of oxygen by carbon atoms cause the rearranging of MoO_3 lattice, thus eliminating vacancies by local collapse. This leads to nucleation and the growth of new phases. From this intermediate state, depending on the reductive conditions, the composition of the reductive flow, pressure and temperature, two phases can be obtained, either MoO_2 or MoO_xC_y [1–3].

On the other hand, after the treatment of MoO_3 with the reductive mixture, the Raman bands at 996 and 820 cm^{-1} decreased in intensity until they completely disappeared, with the formation of one new band at 744 cm^{-1} attributed to the bridging of Mo–O vibrations in the MoO_2 [10,11] (Fig. 2). These changes are associated with the degree of crystallization of the samples and the lower oxygen/metal ratios.

The Mo═O bond distances along the *a*- and *b*-axis are shorter than the Mo–O bond distance along the *c*-axis. The Raman bands at 820 and 996 cm^{-1} can be assigned to the stretching vibration of the terminal Mo═O bonds along the *a*- and *b*-axis [10]. The bridging oxygen (longer bond distances) along the *c*-axis are the most weakly bound oxygens as shown by Mestl et al. [10,12]. This consideration suggests that the preferential generation of oxygen vacancies in the oxide matrix (MoO_3) can be along the *c*-axis, which is also indicated by XRD. Therefore, a displacement of the Mo atom toward the terminal oxygen in the *b*-direction can be expected upon the loss of the bridging oxygen, thus weakening the bond to the terminal oxygen atom along the *a*-axis.

Up to this point, our present results on the structural analysis using X-ray and Raman spectroscopy is in perfect coincidence with previous reports [1,4–6,10,11].

3.1.3. Thermal oxidation process of the MoO_xC_y to MoO_3

The typical thermal profile of the MoO_xC_y, obtained by simultaneous TGA–DTA in dry air, is shown in Figs. 3a and b. In general, two main thermal events can be clearly distinguished. It can be observed that the sample mass increases continuously between 200°C and 500°C and is associated with the oxidation processes of MoO_xC_y and MoO_2 to MoO_3. Both processes can be represented by the following equations:

$$MoO_{3-x}C_{y(s)} + x/2O_{2(g)} + yO_{2(g)} \rightarrow MoO_{3(s)} + yCO_{2(g)}, \quad (I)$$

$$MoO_{2(s)} + 1/2O_{2(g)} \rightarrow MoO_{3(s)}. \quad (II)$$

The formula $MoO_{3-x}C_y$ is adopted for balance convenience; oxygen contributions in the process (I)

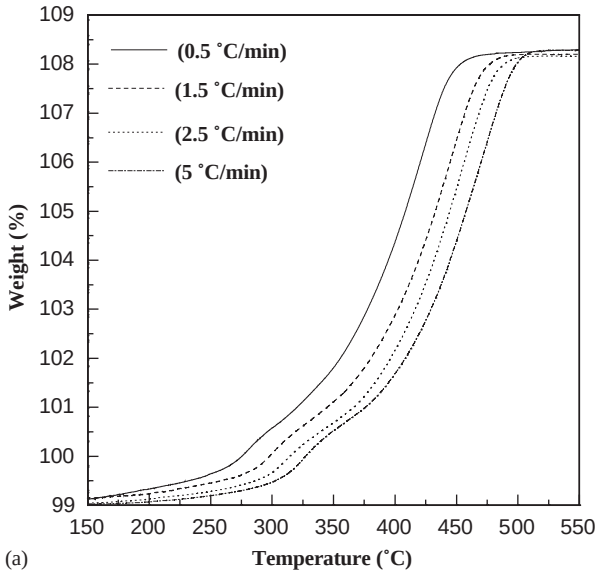

(a)

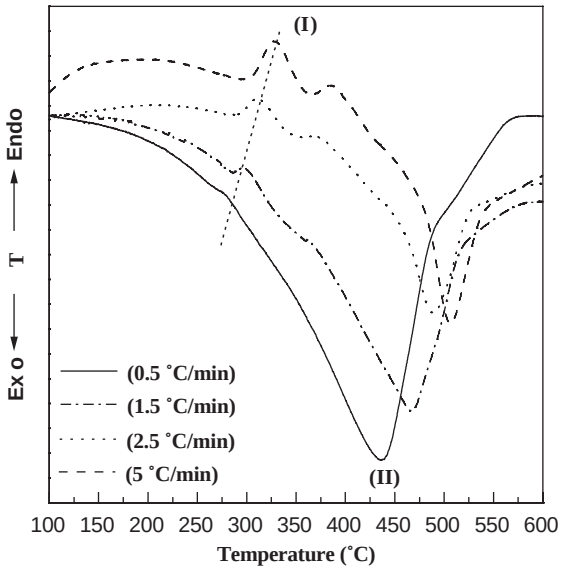

(b)

Fig. 3. (a–b) Typical TGA–DTA curves obtained by conventional thermal analysis for MoO_xC_y (4 h under reducing conditions) are shown.

are separated to visualize its different nature according to the measured dynamic property (weight). One of them (x) implies mass gain and the other (y) is lost as oxidized carbon.

The heat related to the small endothermic effect (I) at around 300°C (Fig. 3b), can be interpreted as the heat necessary to break the interaction of the carbon atoms with the oxide matrix. Segregated carbon is subsequently eliminated in its oxidized form. This endothermic process significantly decreased in intensity and resolution, when the heating rate decreased (see Fig. 3b). The simultaneous mass increase between 200°C and 350°C (Fig. 3a), is associated with oxidation of the residual solid by oxygen.

The exothermic process (II), contiguous to the endothermic event (Fig. 3b), is related to the oxidation process of carbon (to CO or CO_2). The shape and magnitude of this event are also affected by experimental conditions, heating rate and the partial pressure of oxygen. Modifications of these parameters can generate gradients of pressure and temperature which modify the thermal profile and the kinetic parameter.

The weight increase in the range of 350°C and 500°C (Fig. 3a) can be unambiguously related to the oxidation process of MoO_2 to MoO_3, which is accompanied by an approximate mass change of 7.1%, that represents (in accordance with the stoichiometric relations in Eq. (II)) a MoO_2 content in the sample near to 56%.

Following the DTA results, which show that decomposition of the $MoO_{3-x}C_y$ occurs as the first step of its oxidation, the process represented in Eq. (I), can be separated in two steps as follows:

$$MoO_{3-x}C_{y(s)} \rightarrow MoO_{3-x(s)} + yC_{(s)}, \quad \text{(III)}$$

$$MoO_{3-x(s)} + x/2O_{2(g)} \rightarrow MoO_{3(s)}. \quad \text{(IV)}$$

Taking into account the fact that oxygen uptake in process (IV) can be calculated from the TG curve (near to 2%), the simple stoichiometric considerations allows to determine that MoO_{3-x} has the formula $MoO_{2.65}$.

3.1.4. Kinetic study

Finally, the collected TGA data were processed in order to obtain a detailed kinetic study of the evolution of the "carbon-modified MoO_3" structure in the presence of dry air. The results obtained for experiments at different heating rates are presented in Figs. 3a and b. Experimental results were analyzed by model fitting (Eq. (3) and Table 1) and isoconversion methods (Eq. (4)).

Table 1
$f(\alpha)$ functions for most common mechanisms in heterogeneous kinetics [13–16]

Model	Symbol	$f(\alpha)$
One-dimensional diffusion	D1	$\frac{1}{2}\alpha$
Two-dimensional diffusion	D2	$-1/\ln(1-\alpha)$
Three-dimensional diffusion (Jander)	D3	$3(1-\alpha)^{2/3}/2(1-(1-\alpha)^{1/3})$
Three-dimensional diffusion (Ginstring-Brounshtein)	D4	$3/2((1-\alpha)^{-1/3}-1)$
Unimolecular decay	F1	$(1-\alpha)$
Phase boundary controlled	$R_n(1 \leqslant n \leqslant 3)$	$n(1-\alpha)^{1-1/n}$
Nucleation and growth (Avrami-Erofeev)	$A_m(0.5 \leqslant m \leqslant 4)$	$m(1-\alpha)[-\ln(1-\alpha)]^{1-1/m}$

3.2. Mathematical procedure

3.2.1. Model fitting method

The experimental TGA curves were analyzed to evaluate the activation energy and the most probable reaction mechanism. This methodology has been described previously [13,14]. Kinetic analysis of solid-state or heterogeneous process is usually based on a single step kinetic equation. This has been called the governing equation [13]:

$$\frac{d\alpha}{dt} = k(T)f(\alpha) = A\exp\left(\frac{E}{kT}\right)f(\alpha), \quad (1)$$

where T is the temperature, t is the time, α is the extent of reaction, $k(T)$ is the rate constant, $f(\alpha)$ is the reaction model, A is the pre-exponential factor, E is the apparent activation energy, and R is the gas constant. The extent of conversion, $0 \leqslant \alpha \leqslant 1$, is a global parameter typically evaluated from weight loss or increase; in this case, α is the ratio of the weight increase as a function of time to the total weight increase.

In the case of a constant heating rate, $\beta = dT/dt$, the explicit dependence in Eq. (1) is eliminated through the trivial transformation.

$$\frac{d\alpha}{dt} = \frac{A}{\beta}\exp\left(-\frac{E}{kT}\right)f(\alpha). \quad (2)$$

Rearranging the variables and taking logarithms:

$$\ln\left(\frac{d\alpha}{dt}\right) - \ln[f(\alpha)] = \ln\left(\frac{A}{\beta}\right) - \left(\frac{E}{RT}\right). \quad (3)$$

By plotting the left side of Eq. (3) against $1/T$, the activation energy can be obtained from the slope and A from the intercept. The best fitting $f(\alpha)$ model is related to the most probable mechanisms (Table 1 and Refs. [13–16]).

3.2.2. Model-free isoconversion method

The isoconversion principle was applied in order to obtain the dependence $(Ea)_\alpha$ as a function of the degree of transformation (α) of the MoO_xC_y in MoO_3. According to this principle the transformation rate $d\alpha/dt$ at the constant extent of conversion is only a function of temperature and $f(\alpha)$ is independent of the heating rates [15,17]. If the Arrhenius equation is applicable, the following relation can be stated:

$$\left[\frac{d\ln(d\alpha/dt)}{dT^{-1}}\right]_\alpha = -\frac{E_\alpha}{R}, \quad (4)$$

where the subscript α indicates the values of isoconversion, $(\alpha_i)_1 = (\alpha_i)_2 = \cdots(\alpha_i)_n$, for each one of the experiments $(1, 2, \ldots, n)$ and each temperature. This equation corresponds to the slope of Eq. (3), i.e., a plot of $\ln(d\alpha/dt)$ vs. $1/T$. This criterion permits an estimation of $(Ea)_\alpha$ without the assumption of any reaction model, i.e., model-free method.

Model fitting method: Tables 2–5 show the results of the application of $f(\alpha)$ functions (Table 1) and Eq. (3) to the obtained thermogravimetric data. Only the results of the best-fit $f(\alpha)$ models are presented.

The analysis made for the first stage of oxidation from the respective $f(\alpha)$ functions showed that these results, being highly variable, exhibit a strong dependence on the reaction model chosen (Tables 2 and 3). Statistical analysis can identify the three "best" reaction models (D3, D4 and F1), which in this case are statistically equivalent.

On the other hand, the analysis for the second stage of oxidation (Tables 4 and 5) suggest that of the reaction models shown in Table 1, the two-dimensional diffusion (D2) models provide the best fits to experimental data. However, in this case, it is not possible to conclude categorically which model describes the best reaction mechanism.

The results presented in this analysis clearly indicate that it is not possible to conclude unequivocally which

Table 2
Arrhenius parameters for non-isothermal oxidation of MoO_xC_y to MoO_3, obtained from the analysis of Eq. (3)

Model	$dT/dt = 0.5$°C/min				$dT/dt = 1.5$°C/min			
	r	sd	i	E	r	sd	i	E
D1	−0.8389	0.26	13.96	84.7	−0.8374	0.22	10.44	71.9
D2	−0.9206	0.24	21.56	121.6	−0.9255	0.20	17.66	108.6
D3	−0.9616	0.22	29.78	164.9	−0.9652	0.19	25.43	151.2
D4	−0.9539	0.23	27.71	152.6	−0.9579	0.19	23.49	139.4
F1	−0.9706	0.19	14.83	84.8	−0.9712	0.15	11.44	72.7
F2	−0.8203	0.19	8.78	58.6	−0.8141	0.15	5.68	46.7
R2	−0.6972	0.20	4.56	42.2	−0.6639	0.15	1.61	30.3
R3	−0.7990	0.20	7.35	56.4	−0.7965	0.15	4.26	44.4
A2	−0.5095	0.19	1.19	23.8	−0.3554	0.15	−1.49	12.4
A3	−0.0871	0.19	−3.52	3.5	−0.2307	0.15	−5.98	7.7
A4	−0.1637	0.19	−5.96	6.6	−0.4777	0.15	−8.31	17.8

Table 3
Arrhenius parameters for non-isothermal oxidation of MoO_xC_y to MoO_3, obtained from the analysis of Eq. (3)

Model	$dT/dt = 2.5$°C/min				$dT/dt = 5$°C/min			
	r	sd	i	E	r	sd	i	E
D1	−0.8976	0.24	20.61	121.6	−0.9153	0.24	24.42	142.4
D2	−0.9493	0.22	28.76	163.0	−0.9593	0.21	33.11	187.8
D3	−0.9766	0.19	37.58	211.5	−0.9825	0.18	42.55	240.3
D4	−0.9715	0.20	35.33	197.7	−0.9782	0.18	40.12	225.4
F1	−0.9836	0.15	20.59	117.3	−0.9878	0.13	24.28	137.9
F2	−0.9198	0.15	14.00	87.2	−0.9453	0.14	17.30	105.2
R2	−0.8548	0.17	9.72	69.6	−0.8920	0.17	12.81	86.2
R3	−0.9044	0.16	12.71	85.5	−0.9300	0.15	16.00	103.5
A2	−0.7938	0.14	5.64	46.8	−0.8669	0.14	8.40	61.3
A3	−0.5476	0.15	0.48	23.3	−0.7137	0.14	2.93	35.7
A4	−0.3089	0.14	−2.18	11.5	−0.5455	0.14	0.11	22.9

r, correlation coefficient; i, intercept; E, activation energy (kJ/mol).

Table 4
Arrhenius parameters for non–isothermal oxidation of MoO_2 to MoO_3, obtained from the analysis of Eq. (3)

Model	$dT/dt = 0.5$°C/min				$dT/dt = 1.5$°C/min			
	r	sd	i	E	r	sd	i	E
D1	−0.9885	0.14	10.71	86.9	−0.9918	0.12	12.96	102.7
D2	−0.9922	0.13	13.95	106.3	−0.9960	0.09	16.70	125.6
D3	−0.9878	0.21	17.15	129.6	−0.9922	0.17	20.47	153.1
D4	–0.9893	0.19	16.53	123.1	–0.9934	0.14	19.70	145.5
F1	–0.9760	0.20	12.04	89.2	–0.9827	0.17	14.31	105.2
F2	–0.9738	0.18	9.22	76.0	–0.9812	0.15	11.16	89.6
R2	–0.9821	0.12	6.72	66.3	–0.9902	0.10	8.42	78.1
R3	–0.9817	0.15	7.85	73.9	–0.9888	0.12	9.75	87.1
A2	–0.9662	0.16	5.76	57.7	–0.9763	0.13	7.23	67.9
A3	–0.9523	0.15	3.49	47.3	–0.9709	0.12	4.69	55.5
A4	−0.9523	0.14	2.27	42.0	–0.9665	0.11	3.34	49.3

Table 5
Arrhenius parameters for non-isothermal oxidation of MoO_2 to MoO_3, obtained from the analysis of Eq. (3)

Model	$dT/dt = dT/dt = 2.5$°C/min				$dT/dt = 5$°C/min			
	r	sd	i	E	r	sd	i	E
D1	−0.9912	0.12	13.75	108.9	–0.9905	0.12	13.55	110.1
D2	−0.9980	0.07	18.00	134.2	–0.9980	0.06	18.00	137.2
D3	–0.9955	0.13	22.04	164.6	–0.9958	0.12	22.30	169.9
D4	–0.9966	0.10	21.14	156.2	–0.9968	0.10	21.35	160.9
F1	–0.9887	0.14	15.28	112.4	–0.9885	0.13	15.29	115.0
F2	–0.9879	0.12	11.92	95.4	–0.9877	0.12	11.81	96.9
R2	–0.9950	0.07	8.97	82.5	–0.9954	0.06	8.72	82.9
R3	–0.9943	0.08	10.43	92.5	–0.9944	0.08	10.28	93.6
A2	–0.9824	0.10	7.70	71.6	–0.9815	0.10	7.45	71.7
A3	–0.9824	0.09	4.99	58.0	–0.9815	0.08	4.66	57.3
A4	–0.9798	0.08	3.56	51.2	–0.9787	0.08	3.19	50.1

r, correlation coefficient; i, intercept; E, activation energy (kJ/mol).

model satisfactorily describes the reaction mechanism. This problem has been discussed in the literature and an alternative model-free method has been proposed [15,16,18].

Taking into account the limitations of the classical model of mathematical fitting of the $f(\alpha)$ functions to discriminate the kinetic law, it was necessary to compare the activation energy results obtained by this method and the isoconversion method. The best kinetic law would be the one which gives the best correlation coefficient and the best agreement between the activation energy value calculated previously by model fitting

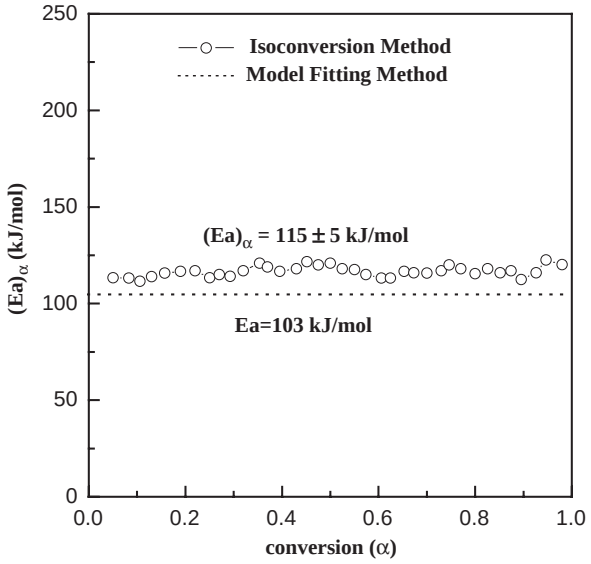

Fig. 4. Dependences of the activation energy on the extent of conversion determined by the isoconversion method (-○-): (---), represent the average value obtained by the model fitting method for the best fits that describes the oxidation process MoO_xC_y to MoO_3 (Unimolecular decay, F1).

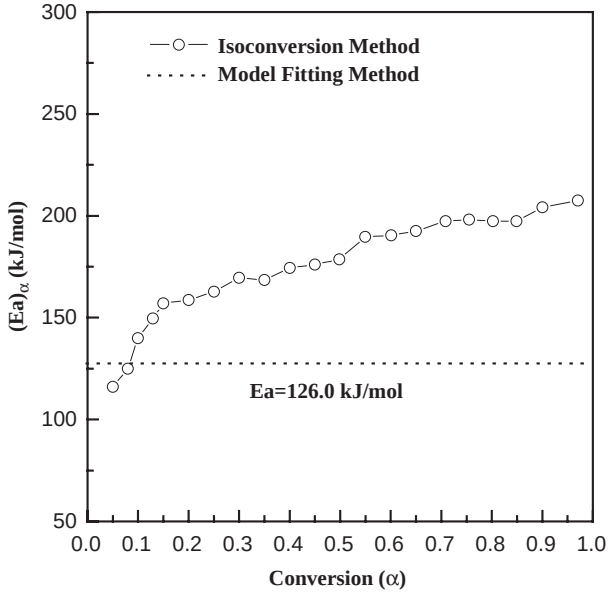

Fig. 5. Dependences of the activation energy on extent of conversion determined by the isoconversion method (-○-): (---), represents the average value obtained by model fitting method for the best fits that describes the oxidation process MoO_2 to MoO_3 (two-dimensional diffusion, D2).

and the value measured directly and independently by the isoconversion method.

Isoconversion method: Figs. 4 and 5 show the obtained results when applying Eq. (4) to a series of TGA experiments performed at different programmed heating rates. This analysis shows that for the first evaluated thermal events the activation energy is independent of the degree of transformation (α) under the experimental conditions used in this study. The results exposed in Fig. 4 suggest that the reaction mechanism during this process is unique; i.e., the step that always limits the speed of the reaction is the same, which, however, does not exclude other simultaneous mechanisms of less importance. The validity of this criterion is confirmed by the fact that the activation energy, which is constant (115 ± 5 kJ/mol) for this process, does not depend on the transformation degree (α) [19].

From an analysis of the results for the first part of the oxidation process, it can be concluded that the most probable mechanism that describes the oxidation of MoO_xC_y to MoO_3 is F1 (unimolecular decay), which presents the best agreement between the activation energy value calculated by model fitting (103 kJ/mol) and isoconversion method (115 kJ/mol), respectively. These results indicate that the reaction is of the first order with respect to oxygen concentration under the experimental conditions used in this study (21% oxygen and dynamic heating rate). Moreover, the fact that the $(Ea)_\alpha$ in this process is constant at any transformation degree, is an evidence of the substitution nature of carbon atoms by oxygen in the MoO_3 matrix. This suggests that substitution occurs in well-defined lattice positions (i.e. energetically equivalent sites).

On the other hand, the stage of the oxidation of the MoO_2 to MoO_3 (Fig. 5) shows that the activation energy rises from about 110 kJ/mol at low conversion to nearly 200 kJ/mol (near the end of the reaction); this range is in agreement with that previously reported [9]. Unlike the model fitting method, which yields a single overall value of activation energy for the whole process (126 kJ/mol), the isoconversion method has the ability to reveal the complexity of the reaction mechanism, in the form of a functional dependence of the activation energy on the extent of conversion. Since the most common situation is the solid-state reactions are not a simple one-step process, analysis of non-isothermal data by the isoconversion method is well suited to reveal this type of complexity that might be discussed in the model fitting kinetic analysis.

The profile of this curve (Fig. 5) shows the different changes of the $(Ea)_\alpha$ as a function of the extent of oxidation (α). These results show a complex $(Ea)_\alpha$ on (α) dependence and reveals typical behavior for competitive reaction, according to Vyazovskin and Wight [15,17]. The variations in the $(Ea)_\alpha$ slope ($\alpha \approx 0.15$) can be associated with a change in the reaction mechanism. Since an isoconversion analysis of non-isothermal oxidation curves is a model-free approach by definition, it does not permit conclusions regarding the reaction mechanism. However, the combined used of the models fitting and isoconversion method can help to predict its kinetic behavior. Taking into account previous criterion

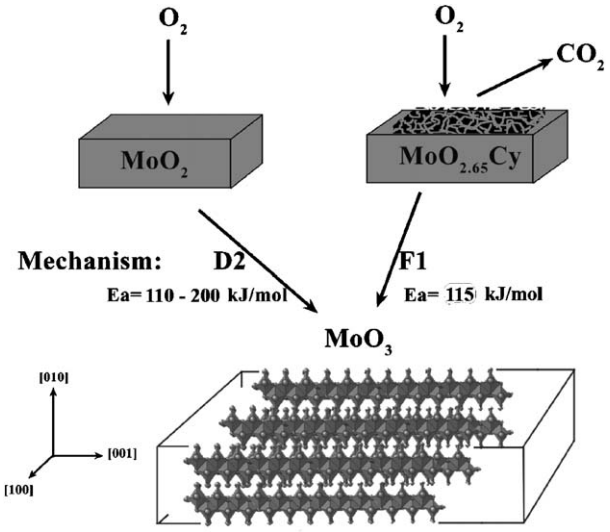

Fig. 6. Schematic representation of the most important oxidation process occurring in MoO_3 reduced sample products (MoO_xC_y and MoO_2).

[16,18] and, analyzing the results obtained by the model fitting and isoconversion method, it can be recognized that the best correlation is for D2 (two-dimensional diffusion) which appears to be the most probable reaction mechanism. The diffusion kinetic model is also consistent with the two-dimensional structural model.

In conclusion, the solid-state kinetic of the oxidation of MoO_2 is governed by two-dimensional diffusion with a variable activation energy value in the range 110–200 kJ/mol, which does not exclude other simultaneous mechanisms, such as three-dimensional diffusion and phase boundary controlled. In the case of molybdenum oxycarbide oxidations appear to take place through a limiting step of the type F1 with well-defined activation energy. A schematic representation of all oxidation processes which occur in a MoO_3 reduced products are summarized in Fig. 6.

A more detailed study for each stage present in this thermal evaluation is difficult because in this interval several simultaneous and complex processes can occur; these can include, bond rupture, adsorption, diffusion, among others. All these considerations make any kinetic study difficult because the possible kinetic evaluation in this temperature interval will have only a global or apparent character without a clear physical or chemical meaning.

4. Conclusions

The following conclusions were drawn from the present study:

The molybdenum oxicarbide was prepared directly from MoO_3 by reductive mixture of $H_2/n\text{-}C_7$ at 370°C. The XRD of the samples obtained show the typical structural transformation of MoO_3 into MoO_xC_y and MoO_2. These structural changes occur preferentially on the [010], [100] and [001] planes, correlated with the changes in intensity and resolution of the Raman bands at 820 and 996 cm^{-1}, when the reaction time increases. This behavior can be related to the degree of cristallinity and reduction of the sample, which may be used to determine the influence of oxygen vacancies have on different molybdenum oxide catalysts.

The kinetic study of the oxidation of "carbon-modified MoO_3" in the temperature range of 150–550°C by simultaneous TGA-DTA was investigated. During the oxidation process two thermal events were detected, which are associated with the breaking bonds, C–Mo–O (endothermic process) because of the presence of carbon by substitution of the oxygen atoms in the bulk structure of the MoO_3 and oxidation of carbon at CO or CO_2 (exothermic process), segregated in the previous endothermic process. Furthermore, the simultaneous oxidation process of the MoO_2 to MoO_3. These thermal events (endothermic and exothermic) occur simultaneously with the oxidation process (TGA curves).

The model-free and model-fitting kinetic approach has been applied to experimental TGA data. The solid state-kinetics of the oxidation of MoO_xC_y to MoO_3 is governed by F1 (unimolecular decay), which suggests that the reaction is of the first order with respect to oxygen concentration. The constant $(Ea)_\alpha$ value (about 115 ± 5 kJ/mol) for this first stage can be related to the nature of the reaction site in the MoO_3 matrix. This suggests that oxidation occurs in a defined lattice position, an energetically equivalent site. On the other hand, for the second stage of oxidation, MoO_2 to MoO_3, the isoconversional analysis shows a complex $(Ea)_\alpha$ on (α) dependence and reveals typical behavior for competitive reaction. A D2 (two-dimensional diffusion) mechanism with a variable activation energy value in the range 110–200 kJ/mol were obtained. It could be interpreted as a limited reaction rate by the inter-layers diffusion of the oxygen in the solid bulk, which does not exclude other simultaneous mechanisms, such as three-dimensional diffusion and phase boundary controlled.

References

[1] P. Delporte, F. Meunier, C. Pham-Huu, Philippe. Vennegues, M.J. Ledoux, J. Guille, Catal. Today 23 (1995) 251–267.
[2] M.J. Ledoux, C. Pham-Huu, P. Delporte, E.A. Blekkan, A.P.E. York, E.G. Derouane, A. Fonseca, Sci., Techno Catal. (1994) 81–86.
[3] M.J. Ledoux, P. Del Gallo, C. Pham-Huu, A.P.E. York, Catal. Today 27 (1996) 145–150.

[4] M.J. Ledoux, F. Meunier, B. Heinrich, C. Pham-Huu, M.E. Harlin, A.O.I. Krause, Appl. Catal. A 181 (1999) 157–170.
[5] P. Delporte, C. Pham-Huu, M.J. Ledoux, Appl. Catal. A 149 (1997) 151–180.
[6] J. Haber, E. Lalik, Catal. Today 33 (1997) 119–137.
[7] Y. Ono, Catal. Today 81 (2003) 3–16.
[8] P. Wehrer, S. Libs, L. Hilaire, Appl. Catal. A 238 (2003) 69–84.
[9] T. Ressler, J. Wienold, R.E. Jentoft, T. Neisius, J. Catal. 210 (2002) 67–83.
[10] M. Dieterle, G. Weinberg, G. Mestl, Phys. Chem. Chem. Phys. 4 (2002) 812–821.
[11] M. Dieterle, G. Mestl, Phys. Chem. Chem. Phys. 4 (2002) 822–826.
[12] G. Mestl, N.F.D. Verbruggen, E. Bosch, H. Knözinger, Langmuir 12 (1996) 2961–2967.
[13] M.E. Brown, D. Dollimore, A.K. Galwey, Reactions in the Solid State. Compressive Chemical Kinetics, Vol. 22, Elsevier, Amsterdam, 1980.
[14] P.J. Haines, Thermal Methods of Analysis Principles, Applications and Problems, Champman & Hall, London, United Kingdom, 1995.
[15] S. Vyazovkin, C.A. Wight, Thermochimica Acta 340–341 (1999) 53–68.
[16] E. Torres García, A. Peláiz Barranco, C. Vázquez, F. Calderón Piñar, O. Pérez Martínez, Thermochimica Acta 372 (2001) 39–44.
[17] S. Vyazovkin, C.A. Wight, Annu. Rev. Phys. Chem. 48 (1997) 125–149.
[18] T. Arii, N. Fujii, J. Analytical, Appl. Pyrolysis 39 (1997) 129–143.
[19] A. Valor, S. Kycia, E. Torres-García, E. Reguera, C. Vázquez-Ramos, F. Sánchez-Sinencio, J. Solid State Chem. 172 (2003) 471–479.